Strain dependence of antiferromagnetic interface coupling in $La_{0.7}Sr_{0.3}MnO_3/SrRuO_3$ superlattices

Sujit Das,[1,2,*] Andreas Herklotz,[1,2,3] Eckhard Pippel,[4] Er Jia Guo,[1,2,5] Diana Rata,[1] and Kathrin Dörr[1,2,†]

[1]*Institute for Physics, MLU Halle-Wittenberg, 06099 Halle, Germany*

[2]*IFW Dresden, Helmholtzstraße 20, 01069 Dresden, Germany*

[3]*Oak Ridge National Laboratory, Oak Ridge, Tennessee 37830, USA*

[4]*Max Planck Institute of Microstructure Physics, Weinberg 2, 06120 Halle, Germany*

[5]*Institute for Physics, Johannes-Gutenberg University Mainz, 55128 Mainz, Germany*

(Received 23 October 2014; revised manuscript received 26 February 2015; published 6 April 2015)

We have investigated the magnetic response of $La_{0.7}Sr_{0.3}MnO_3/SrRuO_3$ superlattices to biaxial in-plane strain applied *in situ*. Superlattices grown on piezoelectric substrates of $0.72PbMg_{1/3}Nb_{2/3}O_3$-$0.28PbTiO_3$(001) (PMN-PT) show strong antiferromagnetic coupling of the two ferromagnetic components. The coupling field of $\mu_0 H_{AF} = 1.8$ T is found to change by $\mu_0 \triangle H_{AF}/\triangle\varepsilon \sim -520$ mT $\%^{-1}$ under reversible biaxial strain $\triangle\varepsilon$ at 80 K in a $[La_{0.7}Sr_{0.3}MnO_3(22\text{Å})/SrRuO_3(55\text{Å})]_{15}$ superlattice. This reveals a significant strain effect on interfacial coupling. The applied in-plane compression enhances the ferromagnetic order in the manganite layers, which are under as-grown tensile strain, leading to a larger net coupling of $SrRuO_3$ layers at the interface. It is thus difficult to disentangle the contributions from strain-dependent antiferromagnetic Mn-O-Ru interface coupling and Mn-O-Mn ferromagnetic double exchange near the interface for the strength of the apparent antiferromagnetic coupling. We discuss our results in the framework of available models.

DOI: 10.1103/PhysRevB.91.134405 PACS number(s): 75.80.+q, 75.47.Lx, 75.70.Ak

I. INTRODUCTION

Magnetic order and coupling at coherent interfaces between oxides of the perovskite type have received increasing interest during the last decade. This includes the search for phenomena already known from metal films, e.g., the exchange bias effect between a ferromagnetic layer and an antiferromagnetic layer [1] and the interlayer coupling through nonmagnetic spacer layers responsible for giant magnetoresistance in Co/Cu/Co [2,3]. Additionally, new phenomena have been discovered that are similar to the two-dimensional electronic states at semiconductor interfaces but add the magnetic degree of freedom to electronic interface states [4]. The most prominent example is the conducting electron gas at the interface between the insulators $LaAlO_3$ and $SrTiO_3$ [5]. The interface of ferromagnetic $SrRuO_3$ (SRO) with ferromagnetic manganites such as $La_{0.7}Sr_{0.3}MnO_3$ (LSMO) is of interest because it shows an antiferromagnetic coupling with thus far unparalleled coupling strength in oxides [6]. The antiferromagnetic exchange coupling at the interface leads to antiparallel orientation of the magnetizations of thin adjacent SRO and LSMO layers which can be sustained in a magnetic field of several teslas [6–8]. The strong reduction of magnetic order at LSMO surfaces or interfaces, termed the "dead layer" in previous work addressed in [9], seems to be weak or absent at the LSMO/SRO interface, as has been shown, e.g., in Ref. [10]. Subsequent work showed the complexity of magnetic order arising from a combination of the antiferromagnetic interface coupling and magnetic anisotropies of the components, which are perpendicular to the film plane and strong for SRO and in plane and weak for LSMO on $SrTiO_3$(001) substrates. An inhomogeneous magnetization depth profile with in-plane Ru spins near the interface and perpendicular Ru spins inside the SRO layer has been detected by neutron reflectivity measurements [11]. The magnetic order at low temperatures depends heavily on the cooling history of the samples [12]. One reason for this is the alignment of Ru spins during cooling through $T_C^{SRO} \sim 150$ K according to the more dominant energy of (i) the exchange coupling to ordered Mn spins ($T_C^{LSMO} \geqslant 250$ K) at the interface, (ii) the magnetic anisotropy energy of SRO, or (iii) the Zeeman energy in an applied magnetic field [12]. At low temperatures, the magnetic anisotropy of SRO is so large that full alignment of Ru spins is hard to achieve in applied magnetic fields of a few teslas. Hence, the arrangement of Ru spins during cooling is (partially) "frozen in."

Meaningful investigation of magnetic coupling at oxide interfaces has been enabled by the advance of experimental tools such as reflection high-energy electron diffraction (RHEED)-assisted layerwise growth under high oxygen pressure [13] and scanning transmission electron microscopy (STEM). The latter allows for semiquantitative evaluation of chemical intermixing at interfaces by applying the high-angle annular dark-field technique (HAADF). Thermal diffuse electron scattering at high angles (>70 mrad) is recorded with the intensity of the localized, incoherent scattering processes proportional to Z^2 (Z denotes the atomic number). Thus, the position of atom columns or individual atoms is imaged with a brightness related to their atomic number, usually referred to as the Z contrast. This technique has been employed to characterize LSMO/SRO interfaces [14,15].

Biaxial epitaxial strain is crucial for magnetic exchange interactions because it systematically alters bond angles and lengths [16]. It has been shown to strongly affect and even reverse the sign of Mn-O-Ru interface coupling in ultrathin $SrRuO_3/AMnO_3/SrRuO_3$ (A = Ca or Pr) trilayers as observed by x-ray magnetic circular dichroism [17]. That experiment revealed the impact of strain on the magnetic coupling by comparing trilayers grown coherently on $SrTiO_3$(001) and $LaAlO_3$(001) substrates. Superlattices (SLs) of LSMO/SRO have not been grown coherently on different substrates thus

*sujitdask@gmail.com

†kathrin.doerr@physik.uni-halle.de

far; rather, all published work has concentrated on SLs grown on TiO_2-terminated $SrTiO_3$(001). Therefore, it seems useful to attempt *in situ* strain control on such SLs using piezoelectric $0.72PbMg_{1/3}Nb_{2/3}O_3$-$0.28PbTiO_3$(001) (PMN-PT) substrates [9,18]. The strain dependence of magnetic order in SRO and LSMO single films was investigated earlier using *in situ* strain [19,20]. Those results for bulklike films with thicknesses beyond 50 unit cells (20 nm) can help us understand the properties of ultrathin layers in SLs but must be considered with care because interfaces do not matter for the magnetization of bulklike films. We investigate the strain dependence of the antiferromagnetic coupling in LSMO/SRO superlattices grown on piezoelectric PMN-PT substrates and find a large response to reversible biaxial strain. The coupling field strongly increases upon reversible in-plane compression, which releases some of the tensile strain in the manganite layers. The observed strain-dependent order of Mn spins at the interface is suggested to contribute to the strain-induced change of the apparent antiferromagnetic coupling.

II. EXPERIMENTS

[22 Å $La_{0.7}Sr_{0.3}MnO_3$(LSMO)/55 Å $SrRuO_3$(SRO)]$_{15}$ SLs have been grown by pulsed laser deposition (PLD) with a KrF laser (wavelength of 248 nm) on (100)-oriented $SrTiO_3$ (STO) and PMN-PT substrates using stoichiometric targets of LSMO and SRO. The laser energy density during deposition was 3 J/cm^2, and the frequency was 3 Hz. The SLs are grown in 0.1 mbar of pure oxygen at 700 °C substrate temperature. After deposition, *in situ* annealing is done at 600 mbar O_2 at 700 °C for 45 min. The deposition started with a LSMO layer and ended with a SRO layer.

The SLs have been structurally characterized by x-ray diffraction in a Bruker D8 Discover diffractometer. The microstructure of the SLs has been investigated by HAADF imaging in a TITAN 80-300 (FEI) STEM. The chemical interdiffusion or intermixing at interfaces was probed by an energy dispersive x-ray spectrometer (EDX) attached to the TITAN operating in the STEM mode. The magnetization of the SLs has been measured using a superconducting quantum interference device magnetometer. The magnetization is expressed in Bohr magnetons per total number of pseudocubic unit cells. The piezoelectric PMN-PT substrates are used to carry out strain-dependent measurements [18,19]. An electrical voltage is applied along the substrate normal between the top of the SL serving as the top electrode and a NiCr/Au back electrode of the substrate. The piezoelectric strain of the substrate is transferred to the SL layers in spite of the large total thickness [9,21]. The magnitude of the substrate strain has been measured using x-ray diffraction at room temperature [21], and the temperature dependence has been reported in Ref. [18].

III. RESULTS AND DISCUSSION

A. Structural characterization

Figure 1(a) shows the θ-2θ x-ray diffraction (XRD) scans around the (002) reflection of the SL grown on PMN-PT and STO. A strong main peak and sharp satellite peaks of the SL are observed, indicating good structural quality with sharp

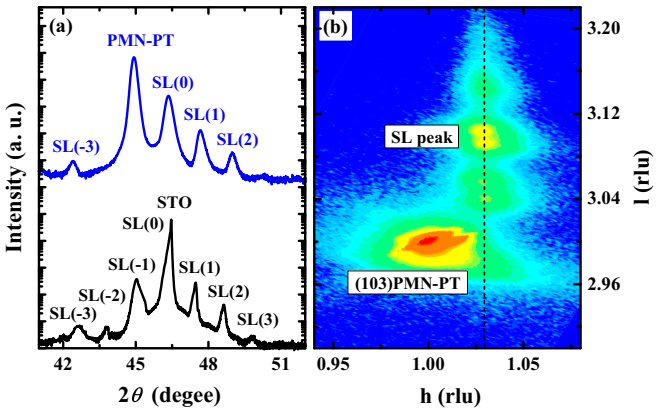

FIG. 1. (Color online) (a) θ-2θ x-ray diffraction scans around the (002) reflection of the superlattices on STO and PMN-PT substrates (b) Reciprocal space map around the (103) reflection on PMN-PT.

interfaces. The differences in peak positions are related to the slightly different in-plane strains of SLs on STO and PMN-PT. In order to determine the average in-plane (a) and the out-of-plane (c) lattice parameters of the superlattices, reciprocal space maps around the pseudocubic (103) reflections were recorded. The determined c lattice parameters of the SL are weighted averages over the components. According to our XRD measurements, SLs grown on STO are strained coherently to the substrate lattice with an in-plane parameter $a_{STO} = 3.905$Å. Thus, the LSMO layers in the coherently grown SL are under tensile strain, while the SRO layers experience compressive strain, referring to the bulk lattice parameters of 3.87 and 3.93 Å for LSMO and SRO, respectively.

An XRD reciprocal space map of the SL on PMN-PT is shown in Fig. 1(b). The SL is not coherently strained to the PMN-PT substrate because of the larger in-plane parameter of $a_{PMN\text{-}PT} \backsimeq 4.02$ Å (which depends on ferroelectric poling). Strain relaxation occurred immediately at the substrate-SL interface where the first LSMO layer forms misfit dislocations. Nevertheless, the SL itself grew coherently with a lattice parameter of $a = 3.92$ Å. This has been checked by high-resolution STEM (see below). Additionally, *in situ* recording of the in-plane parameter by tracking the distance of RHEED diffraction streaks during growth has been used to check for strain relaxation during growth. No strain relaxation has been found, pointing to a coherent growth of the SL. The in-plane lattice parameter of the SL on PMN-PT (3.92 Å) is slightly larger than that on STO (3.905 Å). Hence, LSMO layers are under slightly stronger tensile strain than in the SL grown on STO, while the SRO layers are under very weak compressive strain. To characterize the strain state of the components, we use the in-plane lattice parameter and its deviation from the pseudocubic bulk value (whereas the out-of-plane lattice parameter of the components cannot be determined). In single layers of LSMO or SRO on STO(001) substrates the film structure is expected to be tetragonal (LSMO) or orthorhombic with small monoclinic distortion (SRO), but the symmetry of the layers in the SL might be different. For example, it has been shown that ultrathin SRO layers in SLs with $Pr_{0.7}Ca_{0.3}MnO_3$ layers are tetragonal [22].

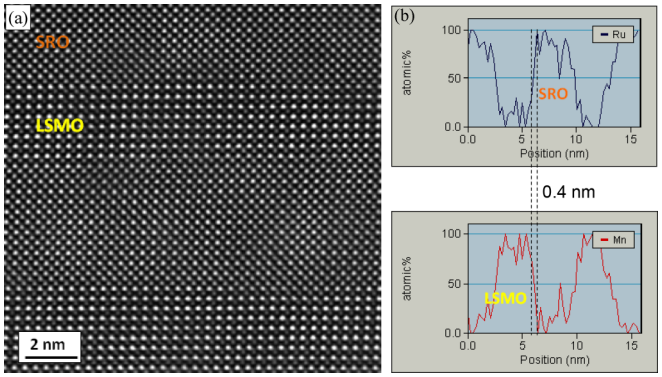

FIG. 2. (Color online) (a) HAADF-STEM images of the investigated SL on PMN-PT and (b) EDX line scans of Ru and Mn, crossing LSMO/SRO layers. The dashed lines indicate an intermixing depth of about 4 Å.

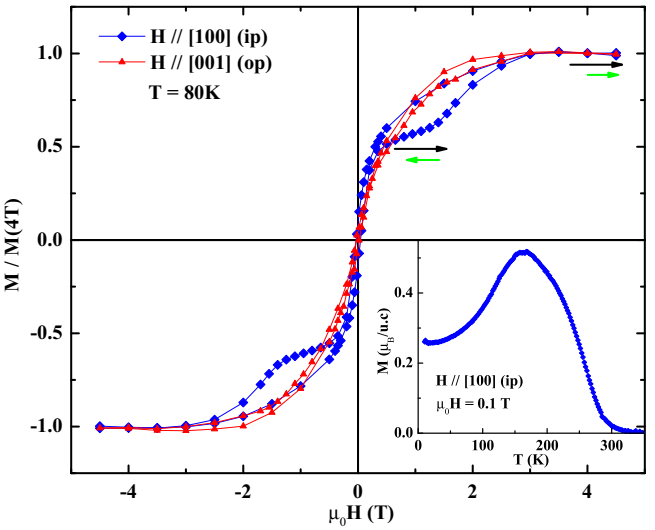

FIG. 3. (Color online) In-plane (ip) and out-of-plane (op) magnetization loops of the superlattice on PMN-PT field cooled at 2 T. Long arrows indicate LSMO magnetization, and short arrows indicate SRO magnetization. The inset shows ip temperature-dependent magnetization at $\mu_0 H = 0.1$ T after field cooling the sample at 2 T.

High-resolution STEM images of the SL on PMN-PT confirm the absence of dislocations and other crystal defects breaking the coherence of the lattice inside the SL [Fig. 2(a)]. Probably because of the less well defined surface of the PMN-PT substrate (and the lattice mismatch of the components), the SRO layers do not grow in a fully flat way and show thickness fluctuations of 2–3 unit cells. The intermixing at the interfaces has been probed by tracking the EDX composition along lines across the interfaces using the Ru $-$ Kα and the Mn-Kα x-ray intensities [Fig. 2(b)]. From Fig. 2(b), the intermixing of the elements Ru and Mn can be deduced to range over a distance of about 1 unit cell for both LSMO/SRO and SRO/LSMO interfaces. Interestingly, intermixing is very small at the interfaces in spite of the nonideal flatness of the layers. This indicates the absence of a chemical driving force for intermixing under the applied growth conditions. No clear difference between the interfaces of LSMO/SRO and SRO/LSMO (in the sequence of growth) has been found, contrary to the expectation for a well-defined termination of sharp interfaces between layers of complete perovskite unit cells. This may result from a random termination on the PMN-PT surface or may be a consequence of the intermixing. An inspection by STEM of a SL on $SrTiO_3$ substrate revealed fully coherent growth of flat layers comparable to that in earlier published work by Ziese *et al.* [6]. A magnitude of intermixing at the interfaces similar to the SL on PMN-PT has been found.

B. Magnetic properties

We first discuss magnetization measurements of a representative SL on PMN-PT. Temperature-dependent in-plane (parallel to the [100] direction) magnetization curves recorded during warming in a moderate magnetic field such as $\mu_0 H = 0.1$ T after field cooling in 2 T give evidence for the antiferromagnetic coupling of SRO and LSMO layers. An example is shown in the inset of Fig. 3, where the total magnetization is the difference of the magnetizations of the components below the Curie temperature of SRO. The Curie temperatures of the components, $T_C^{\mathrm{SRO}} = 156$ K and $T_C^{\mathrm{LSMO}} = 263$ K, are close to the bulk value for SRO and are strongly reduced (because of the tensile strain of $\sim$1.3% and the low layer thickness) for the LSMO layers. Magnetic hysteresis curves $M(H)$ have been measured at temperatures between 10 and 100 K both in the film plane along a pseudocubic [100] direction and along the film normal, the [001] direction. For $T = 80$ K (and in the range of 60–100 K), $M(H)$ reveals hard-axis behavior and nearly reversible magnetization rotation for the normal direction (Fig. 3). This result indicates spontaneous in-plane magnetization for both layers. In-plane $M(H)$ loops measured along a [110] diagonal direction show smaller $M(4\,\mathrm{T})$ and smaller remanent magnetization, both indicating {100} easy axes. (In stating that, we assume biaxial in-plane symmetry is not broken.)

In-plane $M(H)$ loops (Fig. 3) show a two-step switching process in the field. First, the LSMO layers align along the field, followed by the alignment of the SRO layers at 1.8 T. This switching sequence is not immediately obvious because strong antiferromagnetic interlayer coupling may lead to different switching sequences depending on the magnetic moments of both layers [6]. Zeeman energy in the applied field, magnetic anisotropy energy of the respective layers, and interface coupling govern the switching and may lead to different loop shapes and switching sequences [23]. Based on layer thicknesses and ideal magnetization values of $3.7\mu_B$/Mn for LSMO and $1.1\mu_B$/Ru, one expects the magnetic moment of LSMO layers to be larger than that of SRO layers. This would mean, based on magnetization values, that the first switching step is related to LSMO alignment (Fig. 3), whereas the second is the SRO alignment with the applied field. But this argumentation is weakened by the fact that ultrathin strained LSMO layers are not fully ordered and one does not know their magnetization well enough. More confirmation for the switching sequence is found in the strain response, as discussed below. We assign the midpoint of the SRO transition (defined as the point where 50% of the SRO magnetization has been switched) as the coupling field H_{AF}. H_{AF} increases from 1.4 to 2.8 T when the sample is cooled from 100 to

10 K. The magnitude and temperature dependence of H_{AF} are qualitatively similar to those in earlier work on SLs on $SrTiO_3$(001) substrates [7,8] but seem to depend sensitively on the quality of the interfaces. H_{AF} is proportional to the inverse SRO thickness [24] and decreases with an increased level of interface roughness or interdiffusion. Thus far, there is no information on the impact of biaxial in-plane strain on the coupling strength. The observed strong AFM coupling in the SL on PMN-PT indicates good structural interface quality, in agreement with the chemically sharp interfaces found by STEM. The fluctuations in SRO layer thickness surely have the effect of broadening the switching transition. We note that other samples prepared under less favorable growth conditions did not show strong (or even any) coupling; deposition parameters are vital to obtain strongly coupled samples on PMN-PT.

At 10 K, where the anisotropy of SRO is very large, the out-of-plane magnetization is more hysteretic and reveals some remanent magnetization [Fig. 4(a)]. This indicates that some SRO spins are canted out of plane at 10 K. A canted or vertical easy axis may be present in an inner section of the SRO layers [11] at low temperatures. Therefore, strain-dependent measurements have been restricted to $T \geqslant 60$ K, where M essentially lies in the film plane.

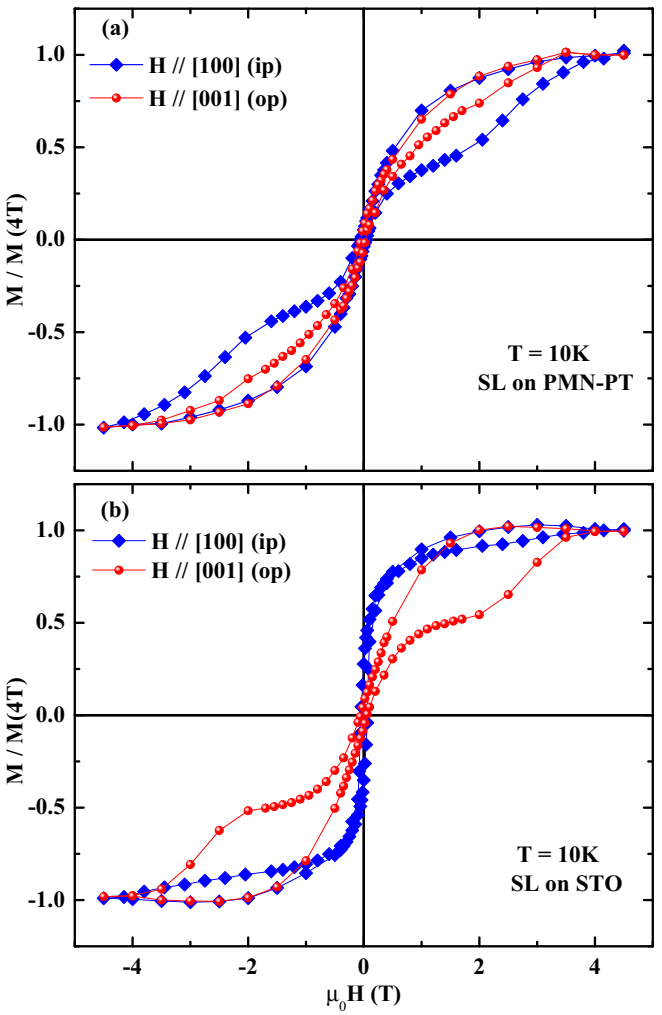

FIG. 4. (Color online) In-plane (ip) and out-of-plane (op) magnetization loops at $T = 10$ K of the superlattices on (a) PMN-PT and (b) STO field cooled at 2 T, respectively.

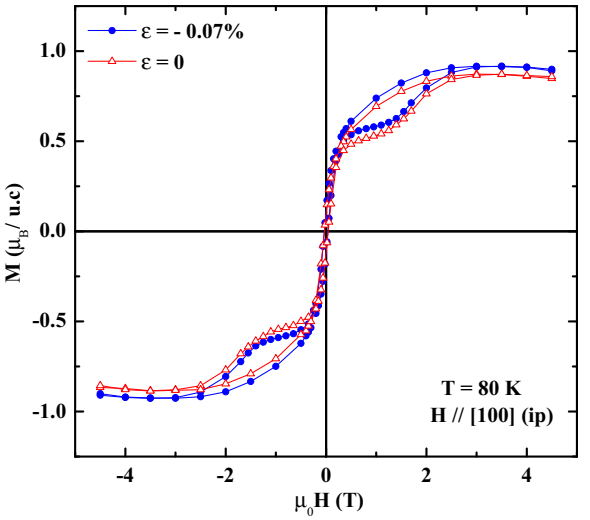

FIG. 5. (Color online) In-plane magnetization loops of the superlattice on PMN-PT in the as-grown state ($\varepsilon = 0$) and after piezocompression ($\varepsilon = -0.07\%$).

To inspect the effect of biaxial strain, Fig. 5 compares the $M(H, T = 80$ K) loops in the as-grown state and a biaxially compressed state ($\triangle\varepsilon \sim -0.07\%$). The change between the two loops is reversible and controlled by the piezoelectric substrate strain. Similar loops have been measured between 60 and 100 K. The immediately obvious impact of the compression is an enlargement of the saturated magnetization (at $\mu_0 H = 4$ T), which roughly agrees with the enlargement seen after the first switching step (at $\mu_0 H = 1$ T; Fig. 5). We note that the strain-induced shift of the transition field is visible only in the expanded view in Fig. 6, which will be discussed later. Ferromagnetic order in LSMO is known to be very sensitive to tensile strain, reflected in strong strain-induced shifts of T_C for thicker LSMO films [19]. Ultrathin LSMO films like those in the present SL sample show some magnetic disorder at the interfaces which substantially reduces the LSMO magnetization. (We estimate an ordered moment of $2.6\mu_B$/Mn below.) The latter fact makes the LSMO magnetization strain dependent through the influence of strain on the ferromagnetic double exchange interaction. The applied reversible compression releases a small part of the as-grown tensile strain of ~1.3% in the LSMO layers. This has a profound effect on LSMO magnetization at $T \ll T_C^{\mathrm{LSMO}}$, which increases by 6.3% (at 60 K), 5.5% (80 K), or 4.4% (100 K). These values have been estimated from the strain-induced magnetization increase observed around 1 T (where SRO is antialigned to LSMO; see Fig. 3) and 4 T (where SRO is aligned parallel to LSMO). As expected for a strain effect on only LSMO, the magnetization increase is the same in both cases. This reveals a general crucial point in assessing the interlayer exchange coupling as an independent parameter of interest because the intralayer magnetic order matters for the observable coupling strength. Stronger apparent AFM coupling of the SRO layer at the interface as detected

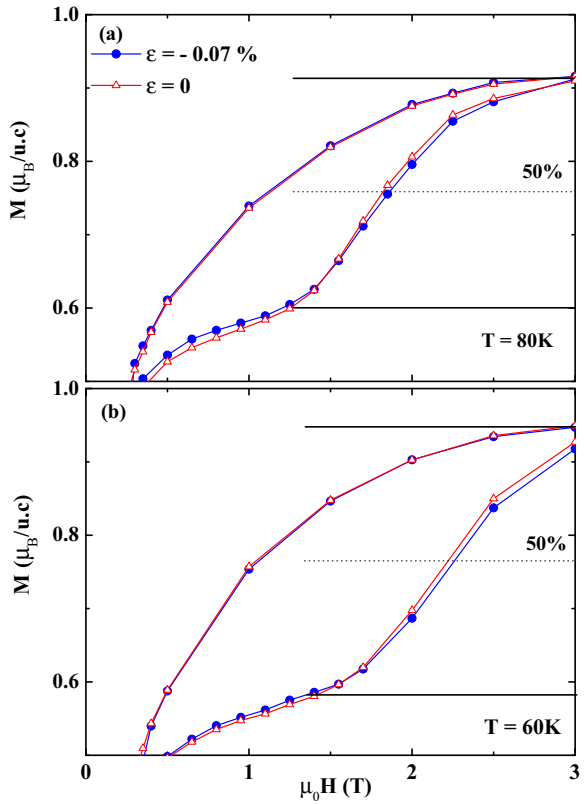

FIG. 6. (Color online) Direct view of the change of antiferromagnetic coupling field H_{AF} induced by the piezocompression at (a) $T = 80$ K and (b) $T = 60$ K. We define H_{AF} as the field where 50% of the SRO magnetization has been switched.

by strain-dependent magnetization measurements may result from both (i) stronger Mn-O-Ru exchange interaction and (ii) a higher-ordered Mn moment at the interface. (We note that the extreme case of randomly oriented Mn moments would offer no net coupling to ferromagnetically aligned Ru moments.) The issue is further discussed below.

Strain-induced changes of H_{AF} have been determined as the difference of H_{AF} values in two investigated strain states. Care has been taken to check the reversibility of the strain-induced change and the reproducibility of the values in several samples and at several temperatures. The two strain states have been measured in immediate sequence, and curves have not been smoothed. Figure 6 provides a direct view on the change of H_{AF} induced by the piezocompression in the following way: the $\varepsilon = 0$ loop has been shifted vertically by a constant value to match the loop under strain at saturation (4 T). In this way, the strain-enhanced LSMO magnetization is compensated. One notes the shift of H_{AF} at the 50% level of the transition. The values are $\mu_0 \triangle H_{AF}/\triangle\varepsilon = -650$, -520, and -410 mT $\%^{-1}$ (with an error of $\sim$20%) at temperatures of 60, 80, and 100 K. (Lower temperatures have not been investigated because the spontaneous magnetization shows some reorientation out of the film plane, as discussed above.) Further, there is a lower slope dM/dH of LSMO around 1 T in the strained case. The latter results from better ferromagnetic order of the LSMO layers after partial release of tensile strain.

The magnetic behavior of the reference SL sample grown on the STO substrate is useful to compare because of its smaller in-plane lattice parameter. The Curie temperatures of the components are $T_C^{\mathrm{SRO}} = 143$ K and $T_C^{\mathrm{LSMO}} = 305$ K. T_C^{SRO} is not very different from the SRO bulk value but is smaller than that of the SL on PMN-PT, in qualitative agreement with the increase of T_C^{SRO} between $a = 3.905$ and 3.92 Å [20]. T_C^{LSMO} is about 40 K higher on STO, an expectable shift for the 0.4% weaker tensile strain of the LSMO layers. The magnetic anisotropies of both SLs are quite different (Fig. 4): curiously, the in-plane and out-of-plane $M(H)$ loops for both cases appear nearly interchanged at 10 K. Weak hysteresis and rotation of magnetization in the field occur for the in-plane $[100_{pc}]$ direction on STO, whereas the out-of-plane M shows a distinct transition at an antiferromagnetic coupling field of $\mu_0 H_{AF} = 2.8$ T. Hence, both layers of LSMO and SRO in the SL on STO have a spontaneous perpendicular (or canted) magnetization which is antiferromagnetically coupled. This coupling has a strength similar to that of the in-plane coupling for the SL on PMN-PT. This change in the magnetic anisotropy is consistent with the known influence of epitaxial strain on the anisotropy in single SRO layers, where compressed films on the STO(001) substrate show tilted perpendicular anisotropy [25].

Regarding the origin of strain-dependent antiferromagnetic coupling, we consider previously reported models. First-principles calculations by Lee *et al.* [26] reveal the lowest total energy for the antiferromagnetic coupling of LSMO and SRO layers for an in-plane lattice parameter close to the one we got on PMN-PT substrates. Similarly, the antiferromagnetic state has been found in density functional theory calculations in Ref. [6]. The influence of in-plane strain has not been investigated yet in such calculations, to our knowledge. On the other hand, the discussion of interface magnetic coupling in oxides has been based on orbital hybridization and strain-dependent orbital occupation in recent work [17,27,28]. For our lattice parameter of 3.92 Å (strong tensile strain of LSMO), Mn e_g orbital energies are split, leading to strong in-plane x^2-y^2 orbital occupation in Mn^{3+} ions. This reduces coupling via the e_g orbitals. The piezocompression releases a small part of tensile strain and enhances the probability of electrons to occupy out-of-plane orbitals ($4d$ t_{2g} xz and yz minority orbitals for Ru, $3d$ e_g $3z^2$-r^2 for Mn). Hence, one would expect stronger hybridization and magnetic coupling under piezocompression, in line with the observed sign of the strain effect on antiferromagnetic coupling. The details in an orbital picture seem to be less clear if one uses previously suggested arguments. Seo *et al.* [17] discussed a strain-dependent orbital occupation of Ru^{4+} ions at interfaces of SRO with various manganites and found a stronger antiferromagnetic coupling for the larger in-plane parameter. This agrees with their experimental results (for different manganites than LSMO) but conflicts with our observation. In a step beyond the consideration in Ref. [17], the contributions of e_g orbitals have been considered. In $SrRuO_3$, the Ru^{4+} e_g orbitals are empty because of the large crystal-field splitting. In Mn^{4+}, they are empty, whereas in Mn^{3+} there is one $e_g^{\uparrow}$ electron. Nominally, LSMO contains 30% Mn^{4+} and 70% Mn^{3+} ions. Coupling via the e_g $3z^2$-r^2 orbitals of Mn and Ru would thus be antiferromagnetic for Mn^{4+}

and ferromagnetic for Mn^{3+} at the interface according to the Goodenough-Kanamori rules. The e_g $3z^2$-r^2 orbital occupation of Mn^{3+} is expected to increase with in-plane compression because the single e_g electron has a higher probability of leaving the tensile-strain-stabilized x^2-y^2 orbital. Again, this e_g-orbital-related mechanism reduces the total antiferromagnetic coupling upon in-plane compression and thus disagrees with our result. Possibly, these single-orbital considerations could not describe the unusually strong antiferromagnetic coupling at the LSMO/SRO interface if it were based on itinerant electrons forming a joined band for both components.

One more option should be considered, which is a nonideal interface structure. Interdiffusion of about 1 unit cell can strongly affect the experimentally observable coupling. Recently, it was shown that Mn ions with a lower oxidation state can even reside on the A site of the ABO_3 perovskite lattice in the case of strong Mn excess [29]. If such a situation were to occur at the LSMO/SRO interface, additional magnetic coupling pathways would be present. Such a mechanism present at nonideal interfaces may also influence experimental results and calls for further improvement of knowledge on real interface structures.

One outcome of this work is the finding that it is difficult to characterize the Mn-O-Ru interface coupling based on magnetization measurements if the Mn-O-Mn coupling at the interface is changing simultaneously. This is clearly true for our experiment, as is seen in the enhanced saturated magnetization of the LSMO layers upon piezocompression. Investigating interface coupling through magnetization measurements means taking into account the intralayer magnetic order in both components as well as the exchange coupling at the interface. Manganite layers are known to show some degree of magnetic disorder at interfaces. In our experiment, this is evident from the lower saturated moment of LSMO as follows. For the as-grown state, the magnetic moment of $\sim 0.6\mu_B$ per unit cell of the superlattice at 1 T is assumed to represent LSMO layers aligned and SRO layers antialigned with the field (Fig. 5). The reversal of SRO layers yields a change of $\sim 0.3\mu_B$ per unit cell, leading to an estimated ordered moment of $2.6\mu_B$/Mn, in contrast to $3.7\mu_B$/Mn for fully ordered Mn spins. The release of tensile strain is known to enhance the ferromagnetic Mn-O-Mn double-exchange interaction in LSMO, in line with the observed larger LSMO magnetization upon in-plane compression. Hence, we expect the increased antiferromagnetic coupling of SRO layers to result partially from better-ordered Mn spins at the interfaces.

IV. CONCLUSIONS

Summarizing, coherent superlattices of [LSMO(22 Å)/SRO(55 Å)]$_{15}$ on piezoelectric PMN-PT substrates show strong antiferromagnetic interface coupling with a profound dependence on reversible strain. The coupling field H_{AF} is enhanced by $\sim$50 mT per 0.1% of reversible biaxial compression (for a superlattice in-plane parameter of 3.92 Å). Simultaneously, the magnetic order of the LSMO layers changes strongly with the strain. We see the latter effect as an important second influence on H_{AF} in addition to the strength of the Mn-O-Ru exchange interaction; it possibly even dominates the observed strain effect. The strain dependence of antiferromagnetic coupling in LSMO/SRO has not yet been understood based on first-principles theory or an orbital hybridization scenario.

ACKNOWLEDGMENTS

This work was supported by the Deutsche Forschungsgemeinschaft (DFG) within the Collaborative Research Center SFB 762 "Functionality of Oxide Interfaces." We thank A. Ernst for discussions.

[1] J. Nogués and I. K. Schuller, J. Magn. Magn. Mater. **192**, 203 (1999).
[2] Z. Q. Qiu, J. Pearson, and S. D. Bader, Phys. Rev. B **46**, 8659 (1992).
[3] P. Bruno and C. Chappert, Phys. Rev. Lett. **67**, 1602 (1991).
[4] H. L. Störmer, R. Dingle, A. C. Gossard, W. Wiegmann, and M. D. Sturge, Solid State Commun. **29**, 705 (1979).
[5] A. Ohtomo and H. Y. Hwang, Nature (London) **427**, 423 (2004).
[6] M. Ziese, I. Vrejoiu, E. Pippel, P. Esquinazi, D. Hesse, C. Etz, J. Henk, A. Ernst, I. V. Maznichenko, W. Hergert, and I. Mertig, Phys. Rev. Lett. **104**, 167203 (2010).
[7] M. Ziese, I. Vrejoiu, and D. Hesse, Appl. Phys. Lett. **97**, 052504 (2010).
[8] M. Ziese, E. Pippel, E. Nikulina, M. Arredondo, and I. Vrejoiu, Nanotechnology **22**, 254025 (2011).
[9] M. C. Dekker, A. Herklotz, L. Schultz, M. Reibold, K. Vogel, M. D. Biegalski, H. M. Christen, and K. Dörr, Phys. Rev. B **84**, 054463 (2011).
[10] M. Ziese, F. Bern, E. Pippel, D. Hesse, and I. Vrejoiu, Nano Lett. **12**, 4276 (2012).
[11] J.-H. Kim, I. Vrejoiu, Y. Khaydukov, T. Keller, J. Stahn, A. Rühm, D. K. Satapathy, V. Hinkov, and B. Keimer, Phys. Rev. B **86**, 180402(R) (2012).
[12] X. Ke, L. J. Belenky, V. Lauter, H. Ambaye, C. W. Bark, C. B. Eom, and M. S. Rzchowski, Phys. Rev. Lett. **110**, 237201 (2013).
[13] G. J. H. M. Rijnders, G. Koster, D. H. A. Blank, and H. Rogalla, Appl. Phys. Lett. **70**, 1888 (1997).
[14] R. Hillebrand, E. Pippel, D. Hesse, I. Vrejoiu, Phys. Status Solidi A **208**, 2144 (2011).
[15] A. Y. Borisevich, A. R. Lupini, J. He, E. A. Eliseev, A. N. Morozovska, G. S. Svechnikov, P. Yu, Y.-H. Chu, R. Ramesh, S. T. Pantelides, S. V. Kalinin, and S. J. Pennycook, Phys. Rev. B **86**, 140102(R) (2012).
[16] S. J. May, J.-W. Kim, J. M. Rondinelli, E. Karapetrova, N. A. Spaldin, A. Bhattacharya, and P. J. Ryan, Phys. Rev. B **82**, 014110 (2010).
[17] J. W. Seo, W. Prellier, P. Padhan, P. Boullay, J.-Y. Kim, H. Lee, C. D. Batista, I. Martin, E. E. M. Chia, T. Wu, B.-G. Cho, and C. Panagopoulos, Phys. Rev. Lett. **105**, 167206 (2010).

[18] A. Herklotz, J. D. Plumhof, A. Rastelli, O. G. Schmidt, L. Schultz and K. Dörr, J. Appl. Phys. **108**, 094101 (2010).
[19] C. Thiele, K. Dörr, O. Bilani, J. Rödel, and L. Schultz, Phys. Rev. B **75**, 054408 (2007).
[20] A. Herklotz, M. Kataja, K. Nenkov, M. D. Biegalski, H.-M. Christen, C. Deneke, L. Schultz, and K. Dörr, Phys. Rev. B **88**, 144412 (2013).
[21] M. D. Biegalski, D.-H. Kim, K. Dörr, and H. M. Christen, Appl. Phys. Lett. **96**, 151905 (2010).
[22] M. Ziese, I. Vrejoiu, E. Pippel, E. Nikulina, and D. Hesse, Appl. Phys. Lett. **98**, 132504 (2011).
[23] A. Solignac, R. Guerrero, P. Gogol, T. Maroutian, F. Ott, L. Largeau, Ph. Lecoeur, and M. Pannetier-Lecoeur, Phys. Rev. Lett. **109**, 027201 (2012).
[24] P. Padhan, W. Prellier, and R. C. Budhani, Appl. Phys. Lett. **88**, 192509 (2006).
[25] M. Ziese, I. Vrejoiu, and D. Hesse, Phys. Rev. B **81**, 184418 (2010).
[26] Y. Lee, B. Caes, and B. N. Harmon, J. Alloys Compd. **450**, 1 (2008).
[27] S. Okamoto, Phys. Rev. B **82**, 024427 (2010).
[28] J. Garcia-Barriocanal, J. C. Cezar, F. Y. Bruno, P. Thakur, N. B. Brookes, C. Utfeld, A. Rivera-Calzada, S. R. Giblin, J. W. Taylor, J. A. Duffy, S. B. Dugdale, T. Nakamura, K. Kodama, C. Leon, S. Okamoto, and J. Santamaria, Nat. Commun. **1**, 82 (2010).
[29] C. Aruta, M. Minola, A. Galdi, R. Ciancio, A. Yu. Petrov, N. B. Brookes, G. Ghiringhelli, L. Maritato, and P. Orgiani, Phys. Rev. B **86**, 115132 (2012).